RSC Advances

ROYAL SOCIETY OF CHEMISTRY

www.rsc.org/advances

Graphical Abstract

High-surface-area Ni/α-Al_2O_3 catalysts exhibit good activity, stability and coking-resistance because high-surface-area support is favorable to the dispersion of Ni.

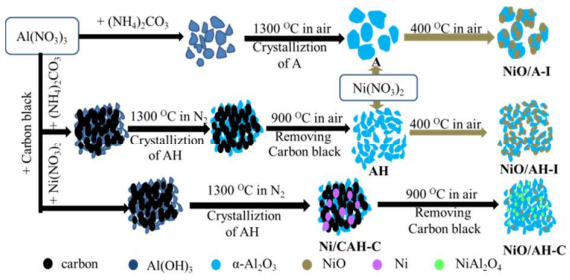

Preparation of high-surface-area Ni/α-Al_2O_3 catalysts for improved CO methanation

Youjun Liu,[a,b] Jiajian Gao,[b] Qing Liu,[b] Fangna Gu,[b,*] Xiaopeng Lu,[a,b]

Lihua Jia,[a,*] Guangwen Xu,[b] Ziyi Zhong,[c] and Fabing Su[b,*]

[a] *College of Chemistry and Chemical Engineering, Qiqihaer University, Qiqihaer161006, Heilongjiang Province, China*

[b] *State Key Laboratory of Multiphase Complex Systems, Institute of Process Engineering, Chinese Academy of Sciences, Beijing 100190, China*

[c] *Institute of Chemical Engineering and Sciences, A*star, 1 Pesek Road, Jurong Island, 627833, Singapore*

*Corresponding author: fngu@ipe.ac.cn (F. Gu), jlh29@163.com (L. Jia), fbsu@ipe.ac.cn (F. Su), Tel.: +86–10–82544850, Fax: +86−10−82544851

Abstract

We have developed a simple approach for preparation of α-Al_2O_3 with high surface area (AH) (about 44 $m^2 \cdot g^{-1}$) through deposition-precipitation of aluminum nitrate on the carbon black hard template. The AH support was impregnated with Ni precursor to obtain the Ni/α-Al_2O_3 catalyst (Ni/AH-I). The above catalyst preparation method was further simplified by one-pot co-precipitation of the nickel and aluminum precursors on the carbon template to obtain AH-supported Ni catalyst (Ni/AH-C). The samples were characterized by nitrogen adsorption, X-ray diffraction, transmission electron microscopy, thermogravimetric analysis, H_2 temperature-programmed reduction and H_2 temperature-programmed desorption. The catalytic test results showed that the both Ni/AH-I and Ni/AH-C catalysts exhibited much more enhanced catalytic performance in syngas methanation than that Ni catalyst supported on low-surface-area α-Al_2O_3 at both atmospheric and high pressures, and at a weight hourly space velocity (WHSV) of 30000 $mL \cdot g^{-1} \cdot h^{-1}$, as well as a good stability in a 50 h high-pressure stability test at an extremely high WHSV of 120000 $mL \cdot g^{-1} \cdot h^{-1}$. The test of accelerated aging indicated that Ni/AH-C showed both better hydrothermal stability and stronger resistance to sintering. This work demonstrates AH can be prepared with high feasibility using carbon black as the hard template, and is suitable as Ni catalyst support for CO methanation.

Keywords: Ni catalyst; high surface area α-Al_2O_3; carbon template; CO methanation; SNG

`

1. Introduction

Recently, production of synthetic natural gas (SNG) from coal- or biomass-derived syngas (H_2 and CO) methanation is proposed for dealing with energy problem.[1-3] In the methanation reaction, Ni-based catalysts are quite attractive and promising because of their relatively fair activity, low cost and high availability as compared to the noble metal catalysts. Among all of the supports, γ-Al_2O_3 is the most commonly used and extensively studied by many researchers due to its developed porous structure and high surface area. However, γ-Al_2O_3 support always suffers from a series of drawbacks, such as phase transformation during the high temperature reaction process[4] which often leads to collapse of the pore structure and burying of the Ni particles. Moreover, the surface acidity of γ-Al_2O_3 support easily causes carbon deposition on the catalyst in syngas methanation,[5-7] together with catalyst sintering and deactivation. Therefore, a lot of efforts have been made to improve the stability of Ni/γ-Al_2O_3, e.g., by adding catalyst promoters,[8-11] or use of advanced catalyst synthesis methods.[12, 13] In addition, some researchers paid their attention to more stable, acid-free and inert α-Al_2O_3 support.[14-16] Zhao et al. investigated La promoted Ni/α-Al_2O_3 catalysts for syngas methanation and found that a proper amount of La could improve both the activity and the stability of Ni/α-Al_2O_3.[17] Gao et al. investigated the influence of different Ni particle sizes in Ni/α-Al_2O_3 on syngas methanation,[18] and demonstrated the feasibility of Ni/α-Al_2O_3 in CO methanation.

As a support, the surface area of α-Al_2O_3 is often less than 10 $m^2 \cdot g^{-1}$,[17, 18] which is too small and restricts the high dispersion of Ni on it. Hence, it is highly desirable to prepare α-Al_2O_3 with large surface area. Several methods have been reported for the preparation of α-Al_2O_3, such as energy intensive ball milling method,[19] hydrothermal synthesis method,[20, 21] and templating method via impregnating γ-Al_2O_3 precursor with a carbon compound followed with three steps of thermal

treatment: carbonization, formation of the α-Al_2O_3 and finally the removal of carbon.[22] However, the surface area of α-Al_2O_3 prepared by these methods is still just 5–15 $m^2 \cdot g^{-1}$. Recently, Pérez et al prepared α-Al_2O_3 with surface area of 16–24 $m^2 \cdot g^{-1}$ using an improved condensation-enhanced self-assembly method.[23] Despite the important progress achieved by this method, however, it is hardly applicable for industrial production considering the constraints of scalability, operability, economy, and safety issues.

Inspired by the method proposed by Santiago et al [24] and along with our previous work,[25] which prepared high surface area hexaaluminate barium using carbon black (CB) as hard template through co-precipitation method, in this work, we prepared α-Al_2O_3 with a high surface area (AH) about 44 $m^2 \cdot g^{-1}$ through a modified co-precipitation method, in which CB was dispersed in ethanol solvent and not removed until the crystalline process. After that, Ni/α-Al_2O_3 catalyst with high surface area was prepared by impregnation method. For the purpose of simplifying the preparation process, the Ni catalysts were also synthesized by the one-pot co-precipitation method, in which the nickel resource and aluminium resource as well as CB were added simultaneously. It was found that the obtained high surface Ni/α-Al_2O_3 catalyst showed higher activity, stability and resistance to carbon deposition. The test of catalytic activity after a high temperature hydrothermal treatment further indicated that the catalyst prepared by the co-precipitation method is more stable than that prepared by the impregnation method. The work provides a feasible way for synthesis of high surface area α-Al_2O_3, which is a promising support not just for the Ni catalysts for SNG production but also for other catalysts that need a very stable support.

2. Experimental

2.1. Preparation of supports and Ni catalysts

Chemicals of analytical grade including aluminum nitrate nonahydrate ($Al(NO_3)_3 \cdot 9H_2O$), ammonium carbonate ($(NH_4)_2CO_3$), and nickel(II) nitrate hexahydrate ($Ni(NO_3)_2 \cdot 6H_2O$) were purchased from Sinopharm Chemical Reagent Co. Ltd., China, and used without further treatment, and CB was from Alfa Aesar (product code 39724, acetylene, 50 % compressed). The schematic diagram of the synthesis process of the support and catalysts is shown in Fig 1. In the synthesis of high surface area α-Al_2O_3 (AH), 75.03 g of $Al(NO_3)_3 \cdot 9H_2O$ was dissolved in 1000 mL of ethyl alcohol at 60 ^oC, followed with addition of 30.00 g CB. The mixture was stirred overnight to get precursor slurry. Likewise, 30.00 g of $(NH_4)_2CO_3$ was dissolved in 400 mL of deionized water and then heated to 60 °C. Subsequently, the $(NH_4)_2CO_3$ solution was added to the above precursor slurry at a controlled pH value at around 8.0, and the resulting mixture was vigorously stirred for 4 h to obtain a gel, which was further filtrated under vacuum and washed with deionized water. The filtered solid was dried at 100 °C overnight, and then calcined in N_2 at 1300 °C for 5 h with a heating rate of 5 °C·min^{-1}, followed by the removal of CB in air at 900 ^oC for 12 h. The obtained high surface area α-Al_2O_3 was denoted as AH. For comparison, an ordinary α-Al_2O_3 was also synthesized by the same method but without addition of CB, and the obtained support was denoted as A.

The Ni catalysts (20 wt% NiO loading) supported on AH and A were prepared by impregnation method. A calculated amount of $Ni(NO_3)_2 \cdot 6H_2O$ was dissolved in 80 mL of distilled water and then 4.0 g of A or AH was added. The mixture was stirred at room temperature for 12 h, and then evaporated at 60 ^oC under stirring to obtain solid samples and dried at 100 °C overnight. After calcination at 400 °C for 5 h in air, the obtained samples were denoted as NiO/AH-I and NiO/A-I, respectively. Accordingly, the catalysts after reduction were denoted as Ni/AH-I and Ni/A-I (I = impregnation).

For simplification of the above preparation process, the catalyst with high surface area was also prepared by one-pot co-precipitation method. 75.03 g of $Al(NO_3)_3 \cdot 9H_2O$ and 9.95 g of $Ni(NO_3)_2 \cdot 6H_2O$ was dissolved in 1000 mL of ethyl alcohol with addition of 30 g CB, followed by precipitating, filtrating, washing, drying and calcining under the same conditions of preparation process of AH. After calcined in N_2 at 1300 °C, the obtained samples was denoted as Ni/CAH-C (Fig 1), and after removal of CB the collected sample was denoted NiO/AH-C. Accordingly, the reduced catalyst was denoted as Ni/AH-C (C = co-precipitation).

2.2. Characterization

X-ray diffraction patterns (XRD) were recorded on a PANalytical X'Pert PRO MPD with a step size of 0.02^o using the Kα radiation of Cu (λ = 1.5418 Å) at 40 kV and 40 mA. The crystal size of the sample was calculated using the Debye-Scherrer equation. Adsorption-desorption isotherms of the samples were measured using N_2 at –196 ^oC with a Quantachrome surface area & pore size analyzer NOVA 3200e. Prior to the measurement, the sample was degassed at 300 ºC for 4 h under vacuum. The specific surface area was determined according to the Brunauer-Emmett-Teller (BET) method in the relative pressure range of 0.05–0.2. The pore-distribution curves (PSD) were calculated with the Barett-Joyner-Halenda (BJH) method using the adsorption isotherm branch. The microscopic feature of the samples was observed by transmission electron microscopy (TEM) (JEM-2010F, JEOL, Tokyo, Japan). Thermogravimetric analysis (TGA) was conducted on a thermogravimetric analyzer TG/DTA 6300 (Seiko Instruments EXSTAR) in air with a flow rate of 100 $mL \cdot min^{-1}$ and a temperature ramp rate of 10 $^oC \cdot min^{-1}$. H_2 temperature-programmed reduction (H_2-TPR) and desorption (H_2-TPD) were carried out on Quantachrome Automated chemisorption analyzer (chemBET pulsar TPR/TPD), and the operation procedures were reported previously.[18] In

the H_2-TPR test, 0.1 g of the sample was loaded in a quartz U-tube and heated from room temperature to 300 ^oC at 10 $^oC \cdot min^{-1}$ and maintained for 1 h under Ar flow. Then the sample was cooled down to room temperature and followed by heating to 1000 ^oC at 10 $^oC \cdot min^{-1}$ in the flow of a binary gas (10.0 vol % H_2/Ar) at 30 $mL \cdot min^{-1}$. In the H_2-TPD experiment, 0.1 g of the catalyst was used and reduced in H_2 flow first. Then the sample was cooled down to room temperature and saturated with H_2. After removing the physically adsorbed H_2 by flushing with Ar for 2 h, the sample was heated to 600 ^oC at a ramping rate of 10 $^oC \cdot min^{-1}$ in Ar flow (30 $mL \cdot min^{-1}$). The released H_2 was detected continuously as a function of increasing temperature using a thermal conductivity detector (TCD). The number of surface Ni sites per unit mass of catalyst was determined by means of H_2-TPD assuming the adsorption stoichiometry of H/Ni=1:1. The peak area of H_2-TPD profile was normalized by that of H_2-TPR of a standard CuO sample.[16] The dispersion of Ni was calculated based on the volume of chemisorbed H_2 using the following simplified equation:[26]

$$D(\%) = \frac{2 \times V_{ad} \times M \times SF}{m \times P \times V_m \times d_r} \times 100$$

where V_{ad} (mL) represents the volume of chemisorbed H_2 under the standard temperature and pressure (STP) conditions measured in the TPD procedure; m is the sample weight (g); M is the atomic weight of Ni (58.69 $g \cdot mol^{-1}$); P is the weight fraction of Ni in the sample as determined by ICP; SF is the stoichiometric factor (the Ni: H molar ratio in the chemisorption) which is taken as 1 and V_m is molar volume of H_2 (22.414 $L \cdot mol^{-1}$) at STP; d_r is the reduction degree of nickel calculated based on H_2-TPR. Hydrothermal treatment for catalysts aging was carried out in a fixed bed quartz tube reactor at 800 ^oC and 0.1 MPa for 7 h with 90 vol % H_2O/H_2 before test, the catalysts after hydrothermal treatment were labeled Ni/AH-I-HT and Ni/AH-C-HT, respectively.

2.3. Catalytic measurement

The catalytic measurements of the catalysts are similar to our previous work.[18] The CO methanation reactions at 0.1 MPa were carried out in a fixed bed quartz tube reactor (ID=8 mm) in the temperature range of 260 to 550 ^{o}C, while that at 3.0 MPa were carried out in a stainless steel reactor nested with a quartz tube (ID=8 mm) in the temperature range of 300 to 550 ^{o}C. Firstly, 0.2 g catalyst (20–40 mesh) was mixed with 5.0 g (2.5 g at high pressures) quartz sand (20–40 mesh) homogenously to avoid the hotspot in bed in the CO methanation. The H_2 and CO reactants as well as N_2 (as an internal standard) were mixed and introduced into the reactor at a molar ratio of $H_2/CO/N_2$ = 3/1/1 and the total flow rate was set to 100 mL·min^{-1} by mass flow controllers. The weight hourly space velocity (WHSV) was 30000 mL (gas) ·g^{-1} (catalyst) ·h^{-1}. The catalyst was reduced at a given temperature in pure H_2 (100 mL·min^{-1}) for 1 h and then cooled down to the starting reaction temperature in H_2 before switching to the reactant gas. The selection of reduction temperature for different catalysts is according to the H_2-TPR results. The outlet gas stream from the reactor was cooled using a cold trap. Inlet and outlet gases were analyzed on line by Micro GC (3000A; Agilent Technologies) after one hour of steady-state operation at each temperature. The concentrations of H_2, N_2, CH_4, and CO in the gas mixture were analyzed by a thermal conductivity detector (TCD) with a Molecular Sieve column while the concentrations of CO_2, C_2H_4, C_2H_6, C_3H_6, and C_3H_8 were analyzed by another TCD with a Plot Q column. Stability test at 3.0 MPa was carried out using the fresh catalysts. After reduced in pure H_2 (100 mL·min^{-1}) for 1 h, the catalyst was cooled down to the reaction temperature and the H_2 flow was changed to the reaction mixture gas to perform the stability test. The CO conversion, CH_4 selectivity and CH_4 yield are defined elsewhere.[27]

The catalytic results are calculated according to the following formulae:

CO conversion: $$X_{CO}\ (\%) = \frac{V_{CO,in} - V_{CO,out}}{V_{CO,in}} \times 100 \quad (1)$$

CH_4 selectivity: $$S_{CH_4}\ (\%) = \frac{V_{CH_4,out}}{V_{CO,in} - V_{CO,out}} \times 100 \quad (2)$$

CH_4 yield: $$Y_{CH_4}\ (\%) = \frac{X_{CO} \cdot S_{CH_4}}{100} = \frac{V_{CH_4,out}}{V_{CO,in}} \times 100 \quad (3)$$

Where $V_{i,\,in}$ and $V_{i,\,out}$ are the volume flow rate of species i (i = CO or CH_4) at inlet and outlet respectively.

The rate and activation energy for CO methanation over the catalyst were determined using the reactor above at 0.1 MPa. 0.5 g catalyst sample (20−40 mesh) diluted with 3.0 g quartz sands (20−40 mesh) was used. The experiments were performed with different total gas flow of 50, 100 and 200 mL·min^{-1} in the temperature range of 230−260 ^{o}C. The rate was determined using the following equation. [28, 29]

$$Rate(r) = \frac{F_{CO} \times X_{CO}}{W} = \frac{X_{CO}}{W/F_{CO}}$$

Where F_{CO} represents the flow of the CO in mmol·s^{-1}, W is the weight of the catalyst in g, and X_{CO} the CO conversion. The variations of X_{CO} with W/F_{CO} were plotted, and then the rates of reaction were calculated at various temperatures from the slope of linear portion. The activation energy was calculated using the Arrhenius equation.

3. Results and discussion

3.1. Characterization of the catalysts

Fig. S1 shows the N_2 adsorption-desorption isotherms (A) and pore-distribution curves (B) of the samples, the hysteresis loop of the samples located at P/P_0=0.8–1.0, indicating the pores in

high-surface-area samples are from the aggradation of nanoparticles, and this agrees with the PSD curves. The surface area of the supports and catalysts are listed in Table 1, the surface area of AH is 44 $m^2 \cdot g^{-1}$, much higher than that of A (0.2 $m^2 \cdot g^{-1}$), demonstrating that adopting CB as template can effectively prevent the agglomeration of particles during the high temperate calcination process, and thus increase the surface area of α-Al_2O_3. After NiO-loading by impregnation, the surface area of NiO/AH-I (39 $m^2 \cdot g^{-1}$) is close to that of α-Al_2O_3 support. Additionally, the surface area of NiO/AH-C is as high as that of NiO/AH-I, suggesting that AH supported Ni catalyst can also be obtained by the one-pot co-precipitation method.

Fig 2a shows the XRD patterns of the supports and the unreduced catalysts. For AH, there are four peaks at 25.7°, 35.4°, 43.6°, and 57.9° corresponding to characteristic planes of α-Al_2O_3 (JCPDS 01-075-0785), and two additional peaks at 31.6°, 32.8° attributing to characteristic planes of θ-Al_2O_3 (JCPDS 01-086-1410), demonstrating the obtained AH is not a very pure phase. The peak intensities of AH is weaker than that of A, possibly because of its smaller particle size. After loading with NiO, some new diffraction peaks at 37.4 °, 43.5 °, and 63.2° can be observed in the patterns of NiO/A-I and NiO/AH-I, which belong to the characteristic peaks of NiO (JCPDS 00-001-1239) (Fig 2a). In contrast, for NiO/AH-C, there are no obvious NiO diffraction peaks. Instead, some new peaks appear at 37.0°, 31.4°, 45.0°, 59.7°, and 65.6°, which come from $NiAl_2O_4$ (JCPDS: 01-073-0239). This agrees with the early reports that NiO can react with Al_2O_3 to form $NiAl_2O_4$ spinel at high temperature,[30] resulting from a strong interaction of NiO particles with Al_2O_3 support. Fig 2b and S2 reveal that all the reduced catalysts show the typical diffraction peaks of metallic Ni (JCPDS 01-070-1849) at 44.5° and 51.8°. In addition, there are no obvious NiO or $NiAl_2O_4$ diffraction peaks in the reduced catalyst, implying that Ni species in the catalysts have been reduced completely. From Fig 2c, it can be seen more clearly that the full width half maximum

(FWHM) of Ni diffraction peaks are obviously different in these catalysts, and Table 1 and S2 list the calculated Ni crystal size of catalysts, which is in the order of Ni/AH-I < Ni/AH-C < Ni/CAH-C < Ni/A-I, implying that Ni crystal size is affected significantly by the surface area of supports and the synthesis method of the catalysts.

Fig 3a shows the H_2-TPR curves of the unreduced catalysts. The reducible NiO species in the catalysts can be approximately classified into three types:[31] α-type (NiO has a weak interaction with support, 310-497 ^oC), β-type (middle interaction, 497-711 ^oC) and γ-type (strong interaction, 711-1000 ^oC). There is one major peak in the H_2-TPR curves of both NiO/AH-I and NiO/A-I. For NiO/A-I, it shows a narrow H_2 consumption peak at 415 ^oC, corresponding to the reduction of α-type NiO. In contrast, NiO/AH-I exhibits a broad and superimposed peak, attributing to the reduction of α-type and β-type NiO respectively, indicating a stronger interaction of NiO with support in this catalyst due to a better dispersion of NiO species on AH support.[31, 32] For the NiO/AH-C catalyst prepared by the co-precipitation method, there are mainly two H_2 consumption peaks at 450 and 900 ^oC, respectively. The former belongs to the superimposed peak of α-type and β-type NiO, while the latter to the reduction of γ-type NiO ($NiAl_2O_4$), as evidenced by the XRD (Fig 2a). This result indicates that the interaction of NiO species with support is further enhanced in the one-pot synthesized NiO/AH-C catalyst.

Fig 3b shows the H_2-TPD profiles of the reduced catalysts. The Ni dispersion is listed in Table 1. The H_2-TPD profile of Ni/A-I shows a weak H_2 desorption peak in the range of 50–300 ^oC, probably because that on the A support the Ni particles are more poorly dispersed. In contrast, Ni/AH-I gives a much stronger peak at 100–200 ^oC, indicating the improved dispersion of Ni on the AH support. Comparing with Ni/AH-I, the H_2 desorption peak of Ni/AH-C shifts slightly toward lower temperature, probably because the higher reduction temperature towards Ni/AH-C decreased

the quantity of its surface defects which can serve as capture traps for surface hydrogen.[33, 34]

Fig 4 shows the TEM images of the supports and reduced catalysts. The A synthesized without CB addition has agglomerated into large particles after calcining at 1300 ^{o}C (Fig 4a). In contrast, the AH prepared by adding carbon black shows irregular and much smaller particle size (Fig 4b) after the high temperature calcination. As shown in Fig 4c-d, the Ni nanoparticles size of Ni/AH-I (10−25nm) is much smaller than that of Ni/A-I (30−120 nm), which is related to the difference of surface area between these two supports. Moreover, the Ni particle size of Ni/CAH-C (Fig S3) is about 80–110 nm, mainly attributed to the Ni sintering caused by the high temperature calcination as high as 1300 ^{o}C in N_2. However, the sintered Ni species can be oxidized to NiO and subsequently react with Al_2O_3 to form $NiAl_2O_4$ ($Ni+1/2O_2 \rightarrow NiO$, $NiO+Al_2O_3 \rightarrow NiAl_2O_4$) during the process of high temperature calcination in air to remove carbon black, as showed in the XRD of Ni/AH-C (Fig 2a). The reduction temperature of spinel is also relative high (950 ^{o}C), but the formation of $NiAl_2O_4$ leads to a higher dispersion of NiO species and stronger interaction of Ni species with the support, which can effectively suppress the sintering and agglomeration of Ni during the reduction process ($NiAl_2O_4+H_2 \rightarrow Ni+Al_2O_3+H_2O$), and even more, the sintering rate of Ni is decreased with the increase of the reduction temperature,[35] leading to smaller Ni particle size or higher Ni dispersion. Thus, for Ni/AH-C (Fig 4e), as we expected, the Ni nanoparticles are still small in size and well dispersed after the reduction. The XRD patterns of Ni/CAH-C and Ni/AH-C (Fig 2a, 2b, S2) further demonstrated this conclusion.

3.2. Catalytic properties of the catalysts

The catalytic activities of the reduced catalysts are distinguished at 0.1 MPa and a weight hourly space velocity (WHSV) of 30000 $mL \cdot g^{-1} \cdot h^{-1}$ and the results are shown in Fig 5a–c and Fig S4a–c.

The CO conversion and CH_4 yield of all the catalysts present volcano-shaped trends with the increase of the reaction temperature, this is because CO methanation is a strongly exothermic reaction and the high temperature has adverse effect on it. The Ni/A-I catalyst shows a poor activity and the maximum CH_4 yield at 450 ^oC is 75%. In contrast, the Ni/AH-I shows a better catalytic activity, especially in the low-temperature range. Its maximum CO conversion and CH_4 yield at 360 ^oC are up to 100 and 87% respectively, most probably related to the higher surface area and smaller Ni particle size in it.[36] Comparing with Ni/AH-I, Ni/AH-C shows a small decrease in the low-temperature activity, but achieves the same activity when the temperature reaches 380 ^oC. For Ni/CAH-C (Fig S4a–c), which is the intermediate materials during the preparation of Ni/AH-C, it shows the poorest activity, probably because it was treated at 1300 ^oC with severely sintered Ni particles.

Considering the SNG production via CO methanation is a volume-reducing and high pressure (2.9–3.4 MPa) process in industry,[37] the catalysts are also tested at 3.0 MPa, and the results are shown in Fig 5e–f and Fig S4e–f. The trend of catalytic activity of all the catalysts is similar to the results of CO methanation at 0.1 MPa. Ni/A-I still shows a poor activity. In contrast, Ni/AH-I shows excellent activity in the low temperature range, and the maximum CO conversion and CH_4 yield can reach 100 and 87% at 400 ^oC, respectively. For Ni/AH-C, it shows a similar activity to that of Ni/AH-I above 450 ^oC. Ni/CAH-C (Fig S4e–f) still shows a poor activity as that at 0.1 MPa. In a word, a high dispersion of Ni nanoparticles from the reduction of NiO/AH-I and NiO/AH-C have led to more active Ni sites for CO methanation and enhanced CO conversion.

The Arrhenius plots of the catalysts are presented in Fig 6. It should be pointed out that we have used only data points with CO conversion levels lower than 55% and in most cases even lower than 40%. The activation energy value of Ni/A-I is estimated to be 102.1 $kJ \cdot mol^{-1}$. In contrast, the

activation energies of Ni/AH-I and Ni/AH-C are quite similar, which are between 81 and 88 $kJ \cdot mol^{-1}$, much lower than that of Ni/A-I. The order of activation energies is in good agreement with the trend of activities of these catalysts in CO methanation (Fig 5).

3.3 Stability test

The stability tests were carried out for Ni/A-I, Ni/AH-I and Ni/AH-C at 3.0 MPa, a relatively high temperature of 550 ^{o}C and a high WHSV of 120000 $mL \cdot g^{-1} \cdot h^{-1}$ for 50 h (Fig 7). Although the WHSV value used in this test is four times of that used in the above activity test (Fig 5), the CO conversion and the CH_4 yield over both Ni/AH-I and Ni/AH-C catalysts still can reach 99.0 % and 89 % respectively and almost maintained at this level in the whole stability tests, indicating these two catalysts are very stable at this reaction condition. In contrast, Ni/A-I shows a poor stability, and the CO conversion and CH_4 yield over it decrease obviously with the increase of the reaction time. In short, the two catalysts with high surface area not only exhibit an enhanced CO methanation activity, but also a good stability.

3.4. Characterization of the spent catalysts

The used catalysts after the 50 h stability test at 3.0 MPa were denoted as Ni/A-I-used, Ni/AH-I-used and Ni/AH-C-used respectively, and characterized by XRD, TG and TEM. Fig 8a shows the XRD patterns of these catalysts. The observation of the SiO_2 diffraction peaks in the patterns of some catalysts is because the added quartz sand was not completely separated after the reaction. For Ni/A-I-used, there is an obvious diffraction peak corresponding to graphitic carbon, which can be confirmed by the latter results of TG and TEM (Fig 8c–d); while for Ni/AH-I-used and Ni/AH-C-used, there is no observation of any diffraction peak corresponding to graphitic

carbon, indicating no graphitic carbon was formed or its amount was too small to be detected. From Fig 8b, it can be seen more clearly that the FWHM of Ni/A-I-used is much narrower than that of Ni/AH-I-used and Ni/AH-C-used. The calculation results (Table 1) reveal that the Ni particle size of Ni/A-I-used is increased obviously compared to that of the fresh one due to the low surface area and the weak interaction of Ni with support; while in the case of Ni/AH-I and Ni/AH-C, the Ni particle size is just slightly increased, indicating a much stronger anti-sintering property of these two catalysts. The amount of carbon deposited on the used catalysts was further measured by TG analysis, and the result is presented in Fig 8c. The carbon content over the used Ni/A-I is up to 24.6 wt%. In contrast, the carbon content over the used Ni/AH-I and Ni/AH-C is just 0.6 and 0.4 wt% respectively, and these values are even lower than our previously reported best results,[31] suggesting these two AH supported Ni catalysts have excellent anti-coking property. The TEM results of the used catalysts (Fig 8d–f) reveal the presence of large amount of carbon whiskers in Ni/A-I-used, consistent with the above TG results, and the sintering of Ni particles in it is also serious and the size of Ni particles is increased to 55–125 nm. In contrast, no obvious carbon whiskers and sintering of Ni particles are observed in the Ni/AH-I-used and Ni/AH-C-used, suggesting the high carbon deposition resistance and good stability.

Considering water steam is one of the byproducts in methanation and the steam is often added to the reactant gas mixture to control the hot spots of catalyst bed and reduce carbon deposition in industry, the hydrothermal stability of the Ni catalysts was thus examined. Fig 9 shows the catalytic properties of Ni/AH-I and Ni/AH-C after the hydrothermal treatment (labeled "HT"). Compared with the fresh catalysts, the catalytic activity of Ni/AH-C-HT is almost maintained unchanged, while that of Ni/AH-I-HT decreased drastically, suggesting that the catalyst prepared by co-precipitation is more stable than that prepared by the impregnation method. This may attribute to

the strong interaction of Ni with support in the catalyst prepared by one-pot co-precipitation method. The TEM images of both catalysts after hydrothermal treatment reveal that the Ni particle of Ni/AH-I-HT (30–80 nm) is much larger than that of Ni/AH-C-HT (20–45 nm) (Fig 10), further suggesting the superior stability of the Ni/AH-C catalyst. In other words, the obvious agglomeration of Ni particle should be main reason for the severe deactivation of Ni/AH-I-HT.

4. Conclusions

In summary, we have demonstrated that adopting CB as template can successfully synthesize AH and supported Ni catalyst through impregnation or one-pot co-precipitation. Compared with the catalyst with small surface area prepared by impregnation, the catalysts with high surface area prepared by impregnation or one-pot co-precipitation show much improved catalytic performance, due to their higher H_2 uptakes, Ni dispersion and smaller Ni particle size. In a 50 h stability test conducted at both high temperature and high pressure with a high WHSV of 120000 $mL \cdot g^{-1} \cdot h^{-1}$, the high-surface-area catalysts exhibit good resistance to both Ni sintering and coke formation because of the improved Ni dispersion and stable, acid-free and inert α-Al_2O_3. The catalytic activity test after high temperature hydrothermal treatment also indicates that the high-surface-area catalyst prepared by co-precipitation is more active and resistant to agglomeration than that prepared by impregnation method. The work provides a feasible method for synthesis of AH, and demonstrates it is a good catalyst support for the Ni catalysts for SNG production.

Acknowledgments

The authors gratefully acknowledge the supports from the National Natural Science Foundation of China (No.21476238), the National Basic Research Program (Nos. 2011CB200906 and

2014CB744306), the National High Technology Research and Development Program 863 (No. SS2015AA050502), and "Strategic Priority Research Program" of the Chinese Academy of Sciences (Nos. XDA07010100 and XDA07010200).

References

1. R. Wang, Y. Li, R. Shi and M. Yang, *J. Mol. Catal. A-Chem.*, 2011, **344**, 122-127.
2. Z. Hou, O. Yokota, T. Tanaka and T. Yashima, *Appl. Catal. A-Gen.* , 2003, **253**, 381-387.
3. N. N. Nichio, M. L. Casella, G. F. Santori, E. N. Ponzi and O. A. Ferretti, *Catal. Today.*, 2000, **62**, 231-240.
4. I. Levin and D. Brandon, *J. Am. Ceram. Soc.*, 1998, **81**, 1995-2012.
5. J. Kopyscinski, T. J. Schildhauer and S. Biollaz, *Chem. Eng. Sci.*, 2011, **66**, 1612-1621.
6. C. H. Bartholomew, R. C. Reuel, *Catal. Rev.* , 1982, **24**, 67-112.
7. M. Andersson, F. Abild-Pedersen, I. Remediakis, T. Bligaard, G. Jones, J. Engbæk, O. Lytken, S. Horch, J. H. Nielsen and J. Sehested, *J. Catal.*, 2008, **255**, 6-19.
8. D. Hu, J. Gao, Y. Ping, L. Jia, P. Gunawan, Z. Zhong, G. Xu, F. Gu and F. Su, *Ind. Eng. Chem. Res.* , 2012, **51**, 4875-4886.
9. D. Hu, J. Gao, Y. Ping, L. Jia, P. Gunawan, Z. Zhong, G. Xu, F. Gu and F. Su, *Ind. Eng. Chem. Res.*, 2012, **51**, 4875-4886.
10. T. Horiuchi, H. Hidaka, T. Fukui, Y. Kubo, M. Horio, K. Suzuki and T. Mori, *Appl. Catal. A-Gen.*, 1998, **167**, 195-202.
11. L. Xu, H. Song and L. Chou, *ACS. Catal.*, 2012, **2**, 1331-1342.
12. G. Van Veen, E. Kruissink, E. Doesburg, J. Ross and L. van Reijen, *React. Kinet. Catal. L.*, 1978, **9**, 143-148.

13. A. Zhao, W. Ying, H. Zhang, H. Ma and D. Fang, *Catal. Commun.*, 2012, **17**, 34-38.

14. G. L. Bezemer, T. J. Remans, A. P. van Bavel and A. I. Dugulan, *J. Am. Chem. Soc.*, 2010, **132**, 8540-8541.

15. J. J. Liu, *Chem Cat.Chem.*, 2011, **3**, 934-948.

16. J. Gao, C. Jia, J. Li, M. Zhang, F. Gu, G. Xu, Z. Zhong and F. Su, *J. Nat. Gas. Chem.* , 2013, **22**, 919-927.

17. A. Zhao, W. Ying, H. Zhang, H. Ma and D. Fang, *Wood Sci. Technol.*, 2011, **59**. 1002-1006

18. J. Gao, C. Jia, M. Zhang, F. Gu, G. Xu and F. Su, *Catal. Sci. Technol.*, 2013, **3**, 2009-2015.

19. G. R. Karagedov and N. Z. Lyakhov, *Nanostruct. Mater.*, 1999, **11**, 559-572.

20. W. L. Suchanek, *J. Am. Ceram. Soc.*, 2010, **93**, 399-412.

21. W. L. Suchanek and J. M. Garcés, *Cryst.Eng.Commum.*, 2010, **12**, 2996-3002.

22. H. Dai, J. Gong, H. Kim and D. Lee, *Nanotechnol.*, 2002, **13**, 674-677.

23. L. L. p. Pérez, V. Zarubina, H. J. Heeres and I. Melián-Cabrera, *Chem. Mater.*, 2013, **25**, 3971-3978.

24. M. Santiago, J. C. Groen and J. Pérez-Ramírez, *J. Catal.*, 2008, **257**, 152-162.

25. J. Gao, C. Jia, M. Zhang, F. Gu, G. Xu, Z. Zhong and F. Su, *RSC Adv.*, 2013, **3**, 18156-18163.

26. C. Jia, J. Gao, J. Li, F. Gu, G. Xu, Z. Zhong and F. Su, *Catal. Sci. Technol.*, 2013, **3**, 490-499.

27. I. Czekaj, F. Loviat, F. Raimondi, J. Wambach, S. Biollaz and A. Wokaun, *Appl. Catal. A-Gen.*, 2007, **329**, 68-78.

28. A. L. Kustov, A. M. Frey, K. E. Larsen, T. Johannessen, J. K. Norskov and C. H. Christensen, *Appl. Catal. A-Gen.*, 2007, **320**, 98-104.

29. V. M. Shinde and G. Madras, *AICHE. J.*, 2014, **60**, 1027-1035.

30. P. Bolt, F. Habraken and J. Geus, *J. Catal.*, 1995, **151**, 300-306.

31. Q. Liu, J. Gao, M. Zhang, H. Li, F. Gu, G. Xu, Z. Zhong and F. Su, *RSC. Adv.*, 2014, **4**, 16094-16103.

32. S. Hwang, J. Lee, U. G. Hong, J. G. Seo, J. C. Jung, D. J. Koh, H. Lim, C. Byun and I. K. Song, *J. Ind. Eng. Chem.*, 2011, **17**, 154-157.

33. P. Djinović, J. Batista and A. Pintar, *Appl. Catal. A-Gen.*, 2008, **347**, 23-33.

34. J. Liu, C. Li, F. Wang, S. He, H. Chen, Y. Zhao, M. Wei, D. G. Evans and X. Duan, *Catal. Sci. Technol.*, 2013, **3**, 2627-2633.

35. C. H. Bartholomew and W. L. Sorensen, *J. Catal.*, 1983, **81**, 131-141.

36. J. Rostrup-Nielsen, K. Pedersen and J. Sehested, *Appl. Catal. A-Gen.* , 2007, **330**, 134-138.

37. J. Gao, Y. Wang, Y. Ping, D. Hu, G. Xu, F. Gu and F. Su, *RSC. Adv.*, 2012, **2**, 2358-2368.

Figure Captions

Fig. 1 Schematic diagram of the formation process of supports and catalysts.

Fig. 2 The XRD patterns of the catalysts: (a) unreduced catalysts and supports, (b) reduced catalysts, and (c) enlarged part of (b).

Fig. 3 (a) H_2-TPR curves of the catalysts and (b) H_2-chemsorption of the reduced catalysts.

Fig. 4 TEM images of the supports and reduced catalysts: (a) A, (b) AH, (c) Ni/A-I, (d) Ni/AH-I, (e) Ni/AH-C.

Fig. 5 Catalytic properties of the catalysts: (a) (d) CO conversion, (b) (e) CH_4 selectivity, and (c) (f) CH_4 yield.

Fig. 6 Arrehnius plots for CO methanation on different Ni catalysts.

Fig. 7 Stability test of the catalysts: (a) CO conversion, (b) CH_4 selectivity, and (c) CH_4 yield.

Fig. 8 (a) the XRD patterns of the used catalysts, (b) enlarged part of (a), (c) the TG of the fresh and used catalysts and (e) (f) (g) the TEM images of the used Ni/A-I, Ni/AH-I and Ni/AH-C catalysts, respectively.

Fig. 9 Catalytic properties of the catalysts after hydrothermal treatment: (a) CO conversion, (b) CH_4 selectivity, and (c) CH_4 yield.

Fig. 10 TEM images of the catalysts after hydrothermal treatment: (a) Ni/AH-I-HT, (b) Ni/AH-C-HT.

Table 1 Physical and chemical properties of the supports and catalysts.

Samples	S_{BET}[a] ($m^2 \cdot g^{-1}$)	Ni particle size (nm)		H_2 uptake ($\mu mol\ g^{-1}$)	D(%)[c]
		by XRD[b]	by TEM		
A	0.2	-	-	-	-
AH	44	-	-	-	-
Ni/A-I	5	34	30-120	9.0	0.7
Ni/AH-I	39	11	10-25	90.0	7.1
Ni/AH-C	40	17	10–30	80.3	6.0
Ni/A-I-used	-	44	55-125	-	-
Ni/AH-I-used	-	14	15-35	-	-
Ni/AH-C-used	-	20	15-30	-	-

[a] surface area, derived from BET equation;

[b] crystal size of Ni, derived from XRD by Debye–Scherrer equation;

[c] Ni dispersion, calculated based on the H_2-TPR and H_2-TPD results.

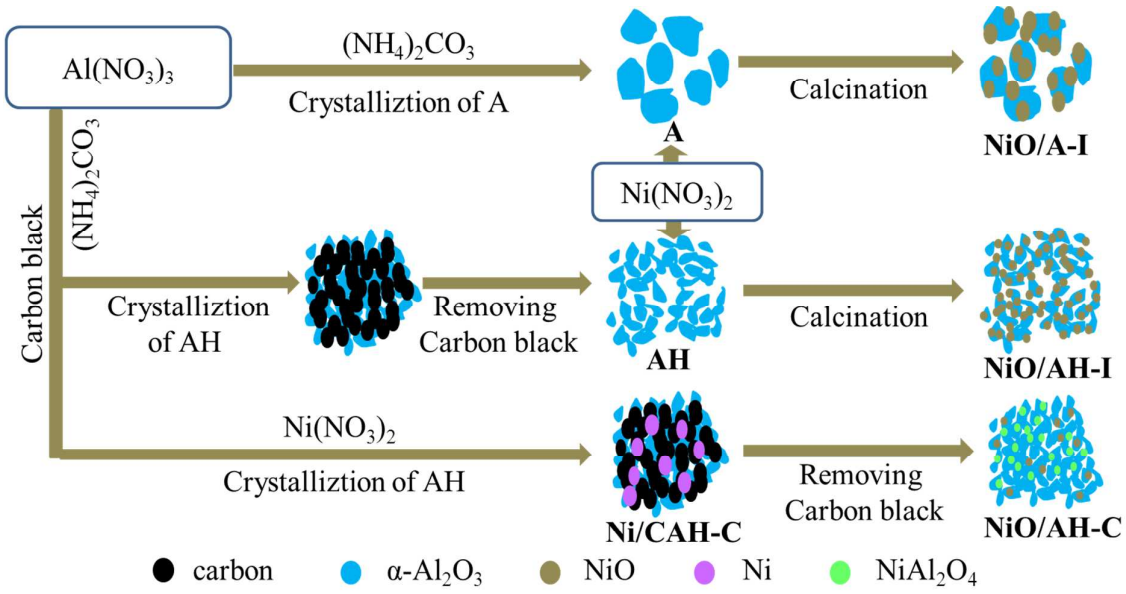

Fig. 1

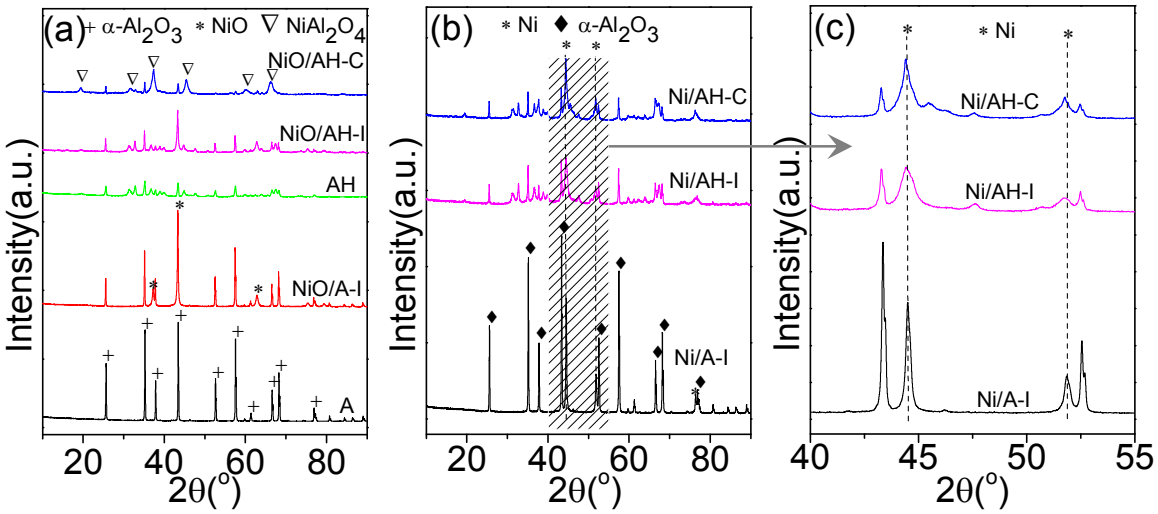

Fig. 2

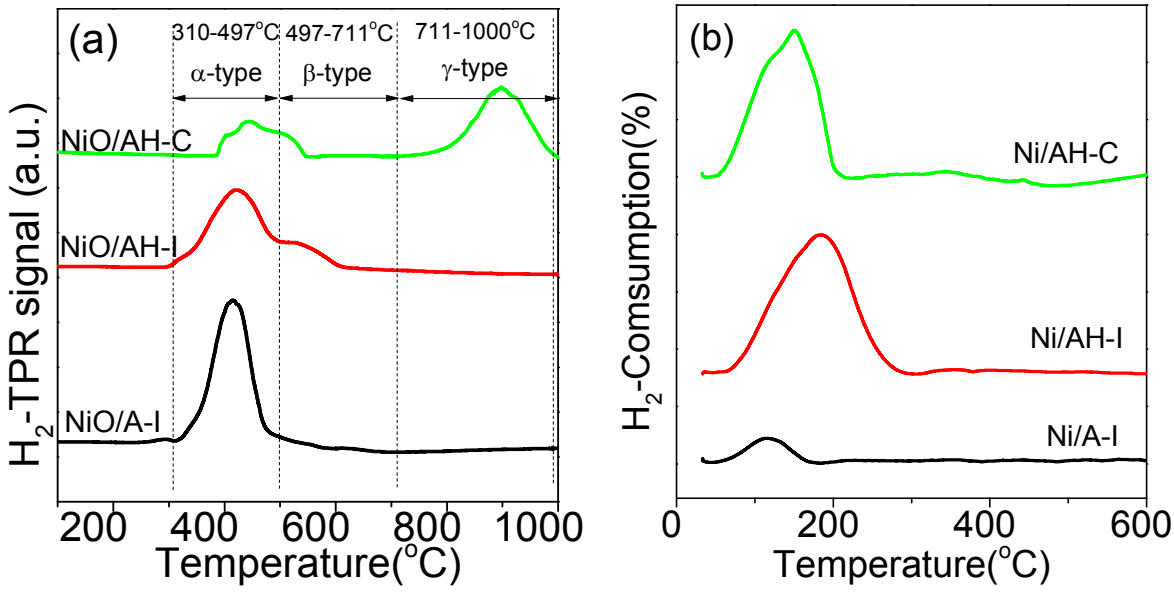

Fig. 3

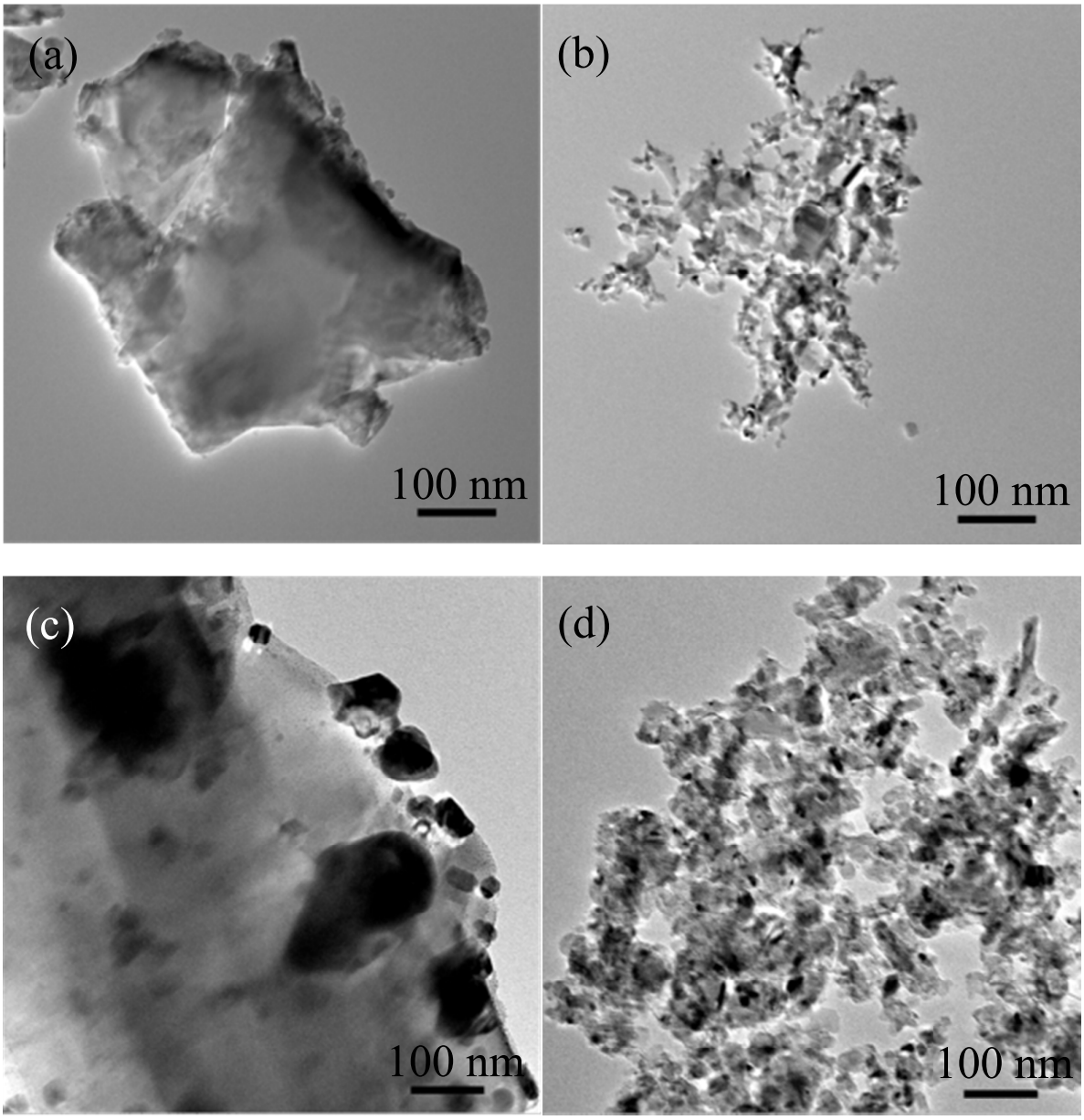

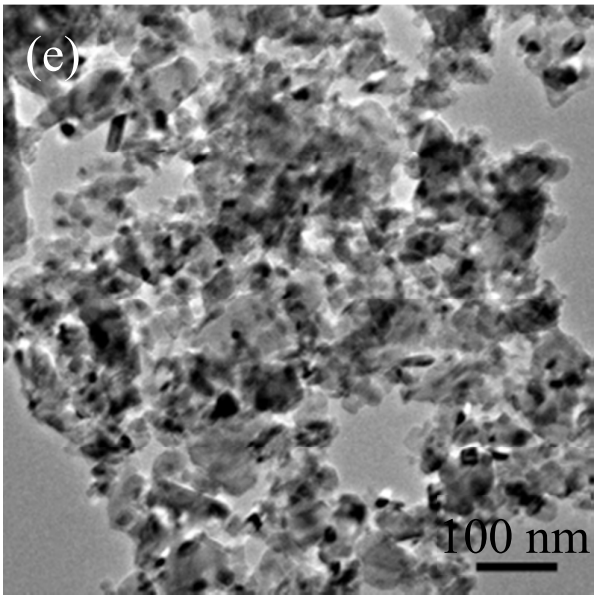

Fig. 4

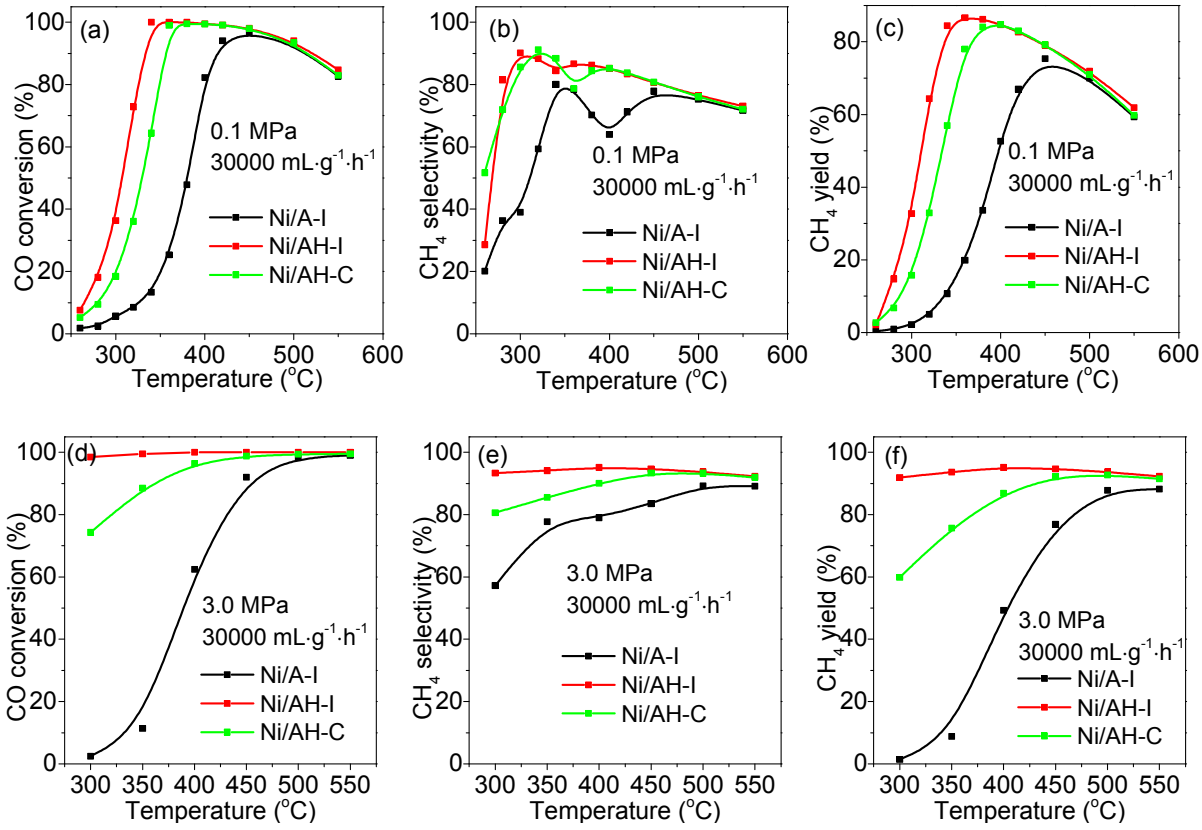

Fig. 5

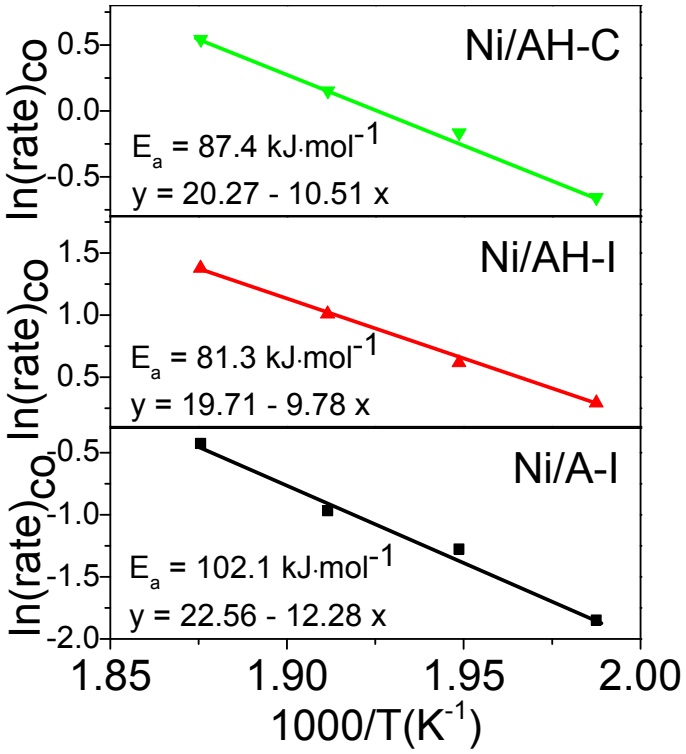

Fig. 6

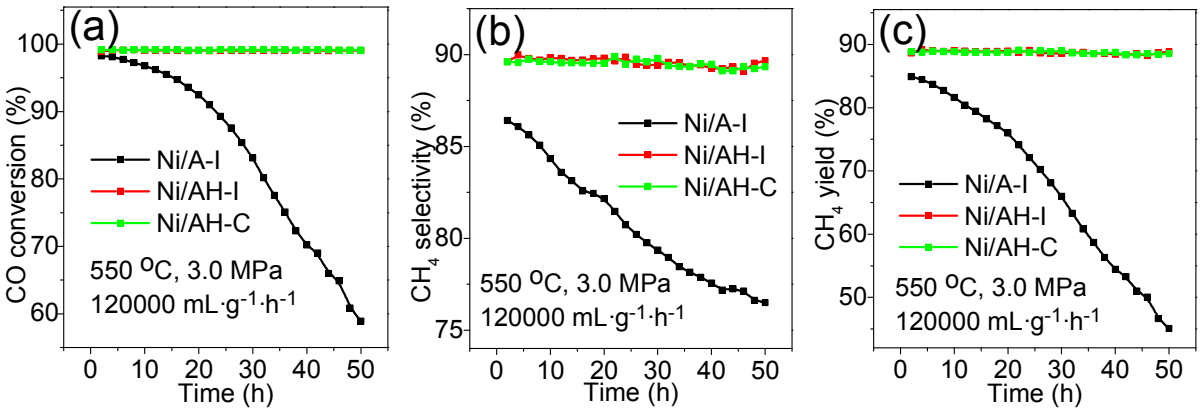

Fig. 7

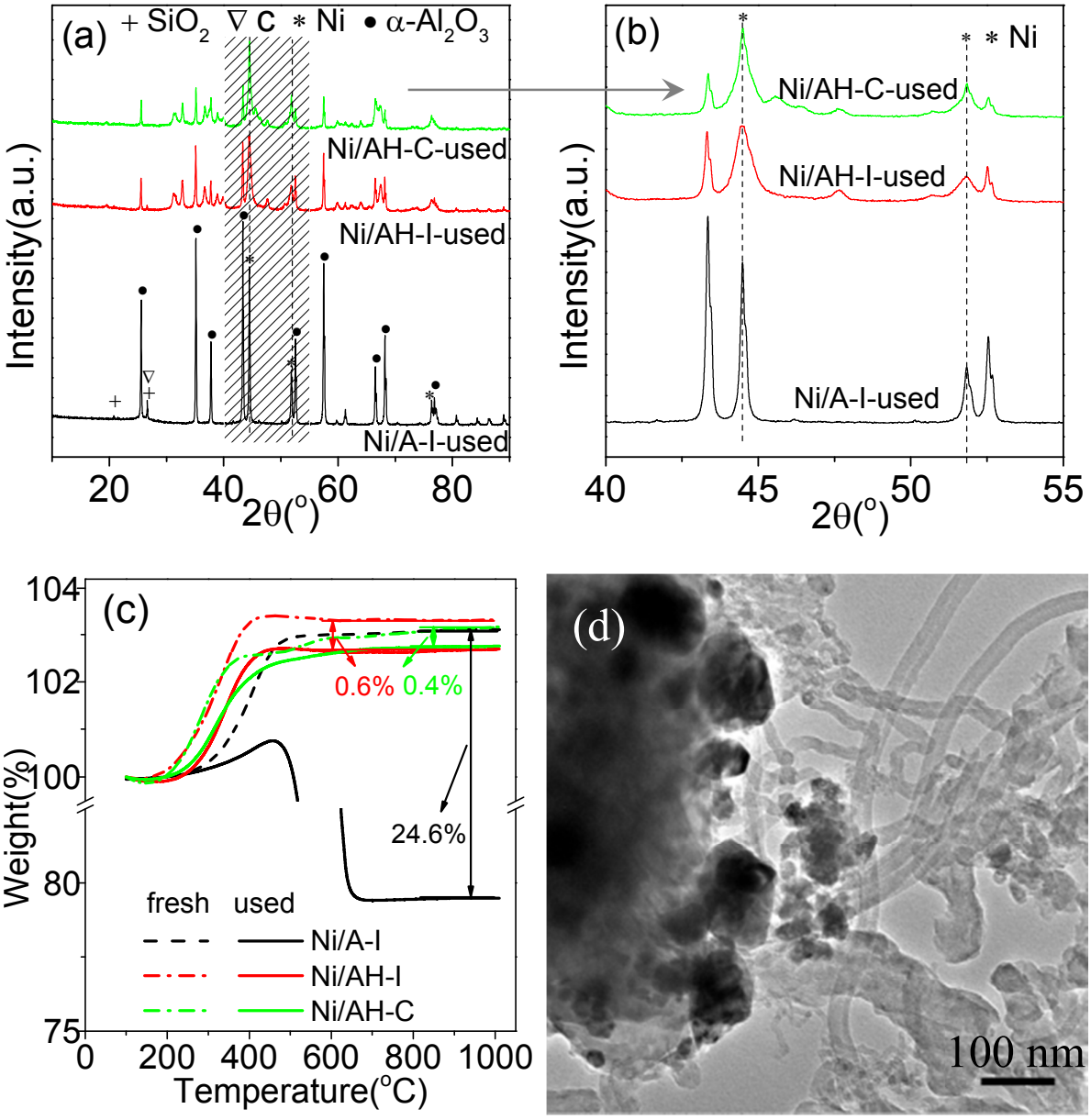

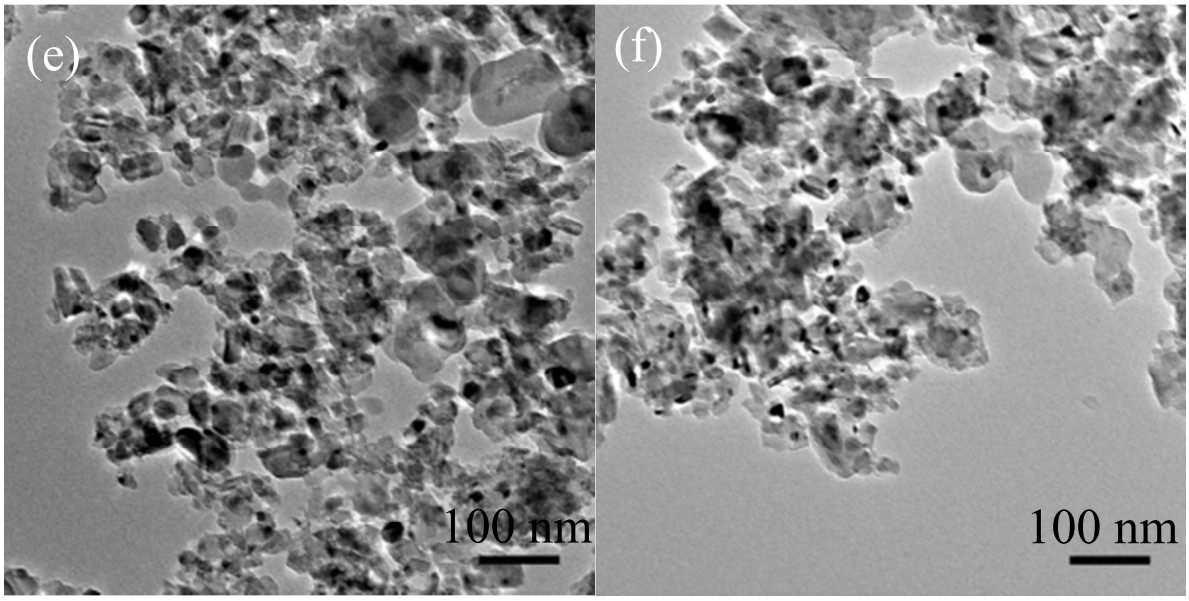

Fig. 8

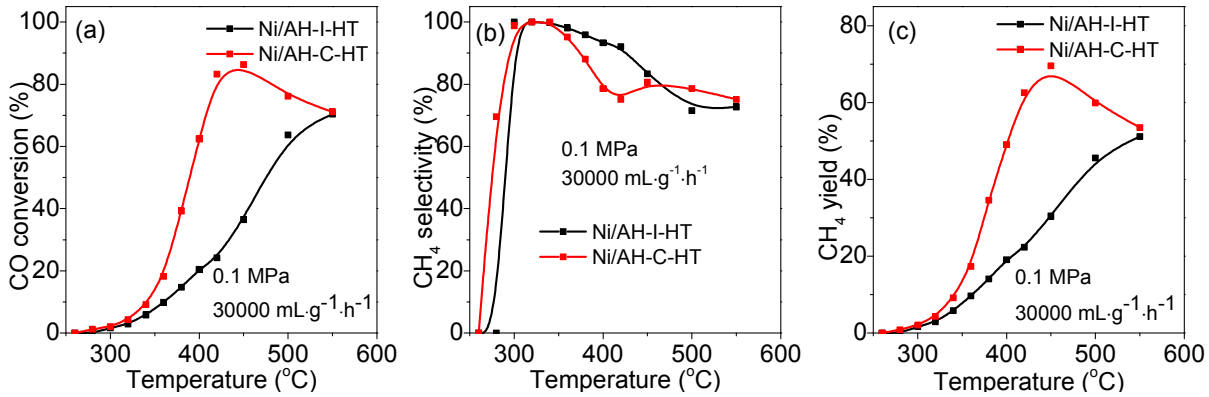

Fig. 9

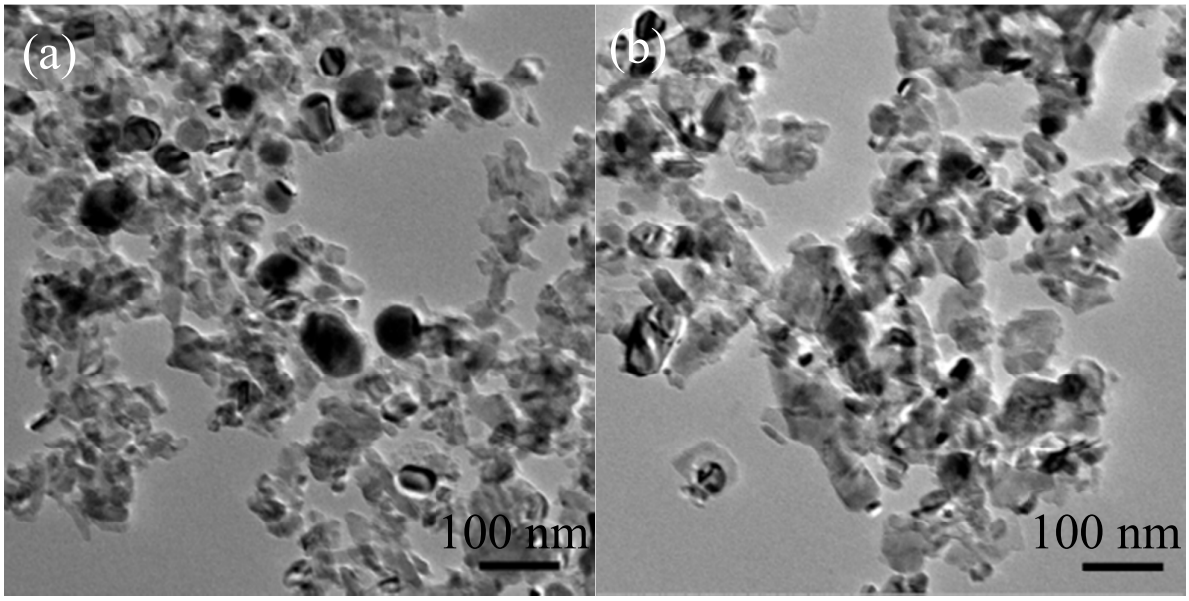

Fig. 10